Evidence of organic matter control on As oxidation by iron oxides in riparian wetlands

Helene Guenet, Mélanie Davranche, Delphine Vantelon, Mathieu Pédrot, Maya Al-Sid-Cheikh, Aline Dia, Jacques Jestin

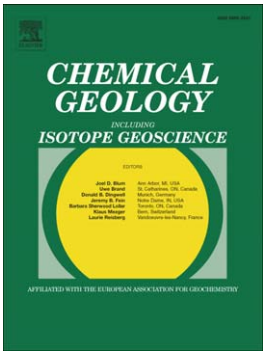

Evidence of organic matter control on As oxidation by iron oxides in riparian wetlands

Helene Guenet, Mélanie Davranche, Delphine Vantelon, Mathieu Pédrot, Maya Al-Sid-Cheikh, Aline Dia, Jacques Jestin

PII: S0009-2541(16)30323-0
DOI: doi: 10.1016/j.chemgeo.2016.06.023
Reference: CHEMGE 17980

To appear in: *Chemical Geology*

Received date: 5 February 2016
Revised date: 20 June 2016
Accepted date: 23 June 2016

Please cite this article as: Guenet, Helene, Davranche, Mélanie, Vantelon, Delphine, Pédrot, Mathieu, Al-Sid-Cheikh, Maya, Dia, Aline, Jestin, Jacques, Evidence of organic matter control on As oxidation by iron oxides in riparian wetlands, *Chemical Geology* (2016), doi: 10.1016/j.chemgeo.2016.06.023

Evidence of organic matter control on As oxidation by iron oxides in riparian wetlands

Helene Guenet[1], Mélanie Davranche[1], Delphine Vantelon[2], Mathieu Pédrot[1], Maya Al-Sid-Cheikh[1], Aline Dia[1], Jacques Jestin[3]

[1]Géosciences Rennes, UMR 6118, Univ. Rennes 1, Campus de Baulieu, 35042, Rennes Cedex, France
[2]Synchrotron SOLEIL, L'orme des merisiers, Saint Aubin BP48, 91192, Gif sur Yvette Cedex, France
[3]Laboratoire Léon Brillouin, UMR12, Bat 563 CEA Saclay, 91191, Gif sur Yvette Cedex, France

Abstract

Soils in riparian wetlands are periodically flooded, resulting in the establishment of reducing conditions and the solubilization of As, subsequently to the reductive dissolution of Fe(III)-oxyhydroxides. When the water level decreases, the wetlands are reoxidized. However, although the behavior of As under the reducing period is well documented, there is a lack of information regarding its behavior during the oxidizing period.

In this study, we investigated As speciation in oxidation products from an initially reduced wetland soil solution recovered from the Naizin-Kervidy riparian wetland (France). The oxidation products were studied using NanoSIMS analysis and synchrotron X-ray techniques. These products were enriched in organic carbon, Fe and As compared with the soil and soil solution. The NanoSIMS analysis showed a colocalization of As and Fe but also revealed the presence of As hotspots where As was either associated with Fe or organic matter (OM). X-ray absorption spectroscopy (XAS) showed that As was sorbed to Fe(III)-oxyhydroxides. The linear combination fitting (LCF) of the As K-edge XANES revealed that As was not totally oxidized (i.e. between 65 and 100% of As(V)). Shell-by-shell fits of the As K-edge EXAFS showed that As formed binuclear edge-sharing ^{2}E ($R_{As\text{-}Fe}$ = 2.74-2.95 Å) and corner-sharing ^{2}C ($R_{As\text{-}Fe}$ = 3.28-3.43 Å) complexes with Fe.

In addition to study of natural samples, oxidized reference samples were analyzed and demonstrated the role of OM on As speciation. The persistence of As(III) was explained by OM control on the As carrying phase during the oxidation, via the formation of nano-lepidocrocite and small Fe-clusters bound to OM. The small size of the Fe phase led to an increased capacity for As adsorption and an increase in ^{2}E sites compared to ^{2}C active sites for As(III) oxidation.

Introduction

Among wetlands, riparian wetlands are of major importance for contaminant (organics, metals, metalloids, etc.) mobility in the environment. In wetlands during high water levels, reducing conditions are established and favor the reductive dissolution of Fe(III)-oxyhydroxides. The biogeochemical cycle of arsenic is strongly dependent on Fe(III)-oxyhydroxides. Their reductive dissolution leads to the release of As(V) along with Fe(II) and organic matter (OM) in the solution (Davranche et al., 2011; Dia et al., 2015; Grybos et al., 2009, 2007; Olivié-Lauquet et al., 2001). Following its solubilization, As(V) is reduced to As(III), generally by autochthonous bacteria (through detoxification or metabolism processes; Dia et al., 2015). Recent studies have shown that, under such reducing conditions, As(III) might be bound to colloidal or particulate OM via thiol (-SH) groups and/or form ternary complexes, OM-Fe(II)-As, with Fe(II) as cationic bridges (Langner et al., 2011; Mikutta and Kretzschmar, 2011, Catrouillet et al., 2014). In the Mekong flood plain (Cambodia), several studies have demonstrated that subsequently to its release and reduction, As(III) is mobile and contaminates the underlying groundwater; these wetlands are thus considered to be a source of As (Fendorf, 2010; Kocar et al., 2008; Polizzotto et al., 2008). However, in riparian wetlands, when the water level decreases, consequently to the decrease in the precipitation volumes and increase in evaporation, the redox conditions become progressively oxidative, and the fate and behavior of As(III) can be questioned. Two possible mechanisms may occur: either As remains bound to OM via thiol groups or metallic bridges or is bound to the newly formed particulate or colloidal Fe(III) minerals. Its oxidation state must be questioned as well; As(III) could be completely or only partially oxidized as As(V). However, few studies have been performed on oxidation products derived from the wetland soil solution to understand their impact on the As speciation. ThomasArrigo et al. (2014) investigated oxidation products from a peatland surface solution. They revealed that As was adsorbed onto poorly crystalline Fe(III)-oxyhydroxides as As(V) and As(III). They linked the presence of As(III) to the reduction of As(V) by freshwater green algae present in the Fe(III)-oxyhydroxides flocs. Peatlands and riparian wetlands have different water regimes. Peatlands are generally permanently flooded (i.e. reducing condition) while riparian wetlands are subjected to seasonal flooding (i.e. alternating redox). These discrepancies are of major importance in terms of the OM qualities (i.e. mostly

humate for riparian wetlands versus fulvate for peatlands) and properties, mineral reduction/oxidation rates, element fluxes, etc. Al-Sid-Cheikh et al. (2015) showed that oxidation products from riparian wetlands are Fe- and organic-rich and are able to concentrate high amounts of As. Through the statistical treatment of NanoSims images and XANES records, they revealed that the As distribution was correlated to the Fe distribution and they highlighted the presence of hot spots highly enriched in As, OM and S but depleted in Fe. They suggested possible interactions between OM, As and S via OM thiol groups. Because the NanoSIMS analysis only shows colocalizations of the elements, detailed spectroscopic investigations are needed to infer the oxidation state and the local coordination environment of As. Because the amount of OM is high in reoxidation compounds (Al-Sid-Cheikh et al., 2015), it should influence the Fe(III)-oxyhydroxide structure and the As oxidation state and speciation.

The purpose of this study was thus dedicated to identify the fate of As when the riparian wetland became oxidized, namely to identify the distribution of the As speciation in oxidation compounds from a naturally poorly As-enriched riparian wetland (Naizin-Kervidy, France). *In-situ* scavenging devices were used to collect the oxidation products subsequent to the water level decrease in the wetland soil (Al-Sid-Cheikh et al., 2015; Belzile et al., 1989). The bulk and microscale distribution and speciation of As and Fe were investigated by coupling NanoSIMS to XAS experiments (µXANES and µEXAFS).

1 Experimental Method

1.1 Field site description and sample collection

Natural samples were recovered from the Mercy riparian wetland of Kervidy-Naizin located in Brittany in western France at 48°00’42.4’’ N and -2°50’20.2’’ E (decimal degrees). This sub-catchment has been monitored since 1991 to investigate the effects of intensive agriculture (corn culture and livestock) on water quality. The hydrological, pedological and geochemical contexts are therefore well documented (Bourrié et al., 1999; Dia et al., 2000; Gruau et al., 2004; Olivié-Lauquet et al., 2001). The maritime temperate climate is characterized by an annual temperature and precipitation of 10.7 °C and 814 mm days^{-1}, respectively. The adjacent stream is ephemeral and does not often flow from the end of August to October. The upper soil

horizon was defined as the organo-mineral horizon (Ah) of a planosol (according to the WRB international classification) which contained (wt%; anhydrous basis) OM (15%), clay (42%), quartz (30%) and Fe(III)-oxyhydroxides (3.5%) (Grybos et al., 2007). The samples were collected using the method described in Al-Sid-Cheikh et al. (2015) with a collecting device inspired from Belzile et al. (1989). Polytetrafluoroethylene (PTFE) sheets (10 x 18 cm, 1.5-mm-thick), wrapped in nylon filters for protection (size pore, 67µm), were inserted into the upper horizon of the wetland soil during the water-saturation period (i.e. when the soil solution was reduced). This material was selected because of its inert characteristic and resistance toward aging (Belzile et al., 1989; Teasdale et al., 1998). Under these reducing conditions, soil Fe(III)-oxyhydroxides were reductively dissolved by autochthonous bacteria in the soil (Dia et al., 2015), which subsequently induced the solubilization of a large amount of Fe(II) and other elements, primarily associated with the Fe(III)-oxyhydroxides, such as metals or metalloids. The increase in pH due to H^+ consumption by the reductive reactions induced the desorption of a large amount of OM from the mineral surfaces (Grybos et al., 2009). The PTFE sheets were inserted under these reduced conditions. When the water table decreased, the soil was progressively water-desaturated. All of the redox-sensitive elements of the reduced soil solution were potentially oxidized, especially Fe(II) which precipitates in the presence of elevated level of OM to produce Fe(III)-OM solids (Al-Sid-Cheikh et al., 2015; Pédrot et al., 2011a). The PTFE sheets mimicked the hydrophobic soil porosity and the oxidation compounds therefore coated their surface. The sheet scavenger method was validated by Al-Sid-Cheikh et al. (2015), who clearly demonstrated that the coated compounds originated from the soil solution. The precipitates on the PTFE device showed an identical rare earth elements (REE) pattern with the wetland soil solution. The REE are strongly adsorbed on OM and Fe(III)oxyhydroxides and allow these compounds to be traced in the environment (Davranche et al., 2011; Grybos et al., 2007; Tang and Johannesson, 2003). An identical REE pattern between the reduced soil solution and oxidation products demonstrated that precipitated solids on the PTFE device originated from the oxidation of the reduced soil solution without any selection which would have induced a fractionation of REE and a modification of the REE pattern. Moreover the

concentrations of Si and Al (indicating the presence of clays) of the precipitates are low and similar to those in the reduced soil solution (Table 2) confirming that the precipitates originated from the soil solution and not from the soil. In the present study, the sheet scavengers were removed from the soil after five hydrological cycles (i.e. five years) which allows us to study the result of all processes occurring during oxidation/reduction cycles in the wetland. Processes including precipitation of diagenetic solids, As adsorption and Fe(III)-oxyhydroxide maturation occurring within the wetland soil are integrated by the sampling method used in this study.

1.2 Chemical analyses

The collected soil samples were dried at 30°C for 72 h, and then sieved to 2 mm. The samples were digested by alkaline fusion using lithium metaborate ($LiBO_2$) flux and analyzed for major and trace elements at the SARM facility (Service d'Analyse des Roches et des Minéraux, Nancy, France). Dissolved organic carbon (DOC) concentrations were measured using an organic carbon analyzer (Shimmadzu TOC-V CSH). The accuracy of the DOC measurements was estimated to be at ± 5% by using a standard solution of potassium hydrogen phthalate. The iron and As concentrations were determined by ICP-MS using an Agilent technologies 7700x at the University of Rennes 1. The samples were pre-digested twice with 14.6 N HNO_3 at 90°C, evaporated to complete dryness and then resolubilized with HNO_3 at 0.37 mol L^{-1} to avoid any interference with the DOC during the analysis. A flux of He was injected in a collision cell to remove interferences from $^{40}Ar^{35}Cl/^{75}As$ and $^{40}Ar^{16}O/^{56}Fe$. Quantitative analyses were performed using a conventional external calibration procedure (seven external standard multi-element solutions, Inorganic Venture, USA). Rhodium-rhenium was added on-line as an internal standard at a concentration level of 300 mg L^{-1} to correct for instrumental drift and possible matrix effects. Calibration curves were calculated from the intensity ratios of the internal standard and the analyzed elements. The international geostandard SLRS-4 was used to control the accuracy and reproducibility of the measurement procedure. The instrumental error on the As and Fe analysis was below 3%. The chemical As and Fe blanks were lower than the detection limits (respectively 0.003 and 0.07 µg L^{-1}) and were thus negligible.

1.3 NanoSIMS sample preparation and data acquisition

Adhesive carbon tapes were used to recover the coated solid layer from the sheet scavengers. The carbon tapes were analyzed without any other NanoSIMS preparation. Measurements were performed with the Cameca NanoSIMS 50 at the facility at the University of Rennes 1 (France). By using a primary cesium beam (Cs^+; beam current ~15 pA), secondary ions of Fe (as $^{56}Fe^{16}O^-$), carbon (measured as the $^{12}C/^{14}N^-$ ratio to distinguish the carbon of the sample from the one on the scotch tape), and As (as $^{75}As^-$) were sputtered from the sample surface and detected simultaneously (multicollection mode) in electron multipliers at a mass-resolving power of ~4000 (M/ΔM). The primary beam was focused to a spot size of 100 nm and scanned in a raster pattern on the surface sample. The chemical maps were determined by image processing using the ImageJ software (1.38x version) and the NRIMS ImageJ analysis module. The colocalization analyses were performed under JACoP, a plug-in for ImageJ developed by Bolte and Cordelieres (2006). Pearson's coefficient (PC) was calculated to determine the dependency of the pixels in the dual-channel images. PC is a coefficient where 1 and –1 represent a perfect colocalization and perfect exclusion, respectively, and where 0 represents a random colocalization. Manders' coefficients (M1 and M2) were also used for the colocalization studies and can be used to determine the proportion of overlap of each channel with the other. In this case, 1 represents a perfect colocalization and 0 represents no colocalization (Manders et al., 1993). M1 and M2 are insensitive to the intensity of the overlapping pixels, which is convenient when the intensities in both channels have very different values between them, like between Fe and As.

1.4 Reference samples for X-ray absorption spectroscopy

All of the aqueous solutions were prepared with analytical grade Milli-Q water (Millipore). The Fe(II) stock solutions were prepared with iron chloride tetrahydrate ($FeCl_2.4H_2O$) from Acros Organics. The As(III) stock solutions were prepared with a sodium arsenite solution (Na_2AsO_2) from Fluka Analytical. The As(V) stock solution was prepared with arsenate oxide (As_2O_5) from Inorganic Ventures. The synthesis of the organic As-Fe reference compounds was performed at Geosciences Rennes. The OM used was a humic acid (HA) corresponding to Leonardite humic acid (IHSS). The composition of HA was (as a mass fraction): C = 63.81%, O = 31.27%, H = 3.70%, N = 1.23%. The DOC/As and DOC/Fe ratios of the synthesized reference compounds

were representative of the natural reduced soil solution ratios from the studied wetland (Dia et al., 2000; Olivié-Lauquet et al., 2001). The anoxic synthesis of the references was performed inside a Jacomex isolator glove box (< 10 mg L^{-1} of O_2). The pH of the references synthesized from humic acid was set to 6.5 and the ionic strength to 5 10^{-3} mol L^{-1} with NaCl as the electrolyte. A summary of the reference materials and their synthesis is presented in Table 1. HA-As(III)*oxic* was synthesized inside the glovebox from 30 mL of a 648.7 mg L^{-1} Leonardite suspension to which 0.2 mL of a 83 mg L^{-1} Na_2AsO_2 stock solution was added. The concentration of As was 0.55 mg L^{-1}. The suspension was stirred for 24 hours to allow elemental diffusion and prevent decantation (Catrouillet et al., 2015; Hoffmann et al., 2012), and then oxidized outside the glovebox at room temperature until dryness was obtained (approximately one week before analysis). For HA-Fe-As(III)*oxic*, 638 mg L^{-1} HA suspension was deoxygenated in a Jacomex isolator glove box (< 10 ppm of O_2) for 24 hours. In 50 mL of this suspension, 0.3 mL of a 83 mg L^{-1} Na_2AsO_2 stock solution and 6.7 mL of a 950 mg L^{-1} Fe(II) stock solution were added. The final concentrations of DOC, Fe and As were respectively 562.4, 112.5 and 0.49 mg L^{-1}. The suspension was continuously stirred for 24 hours to reach equilibrium and then oxidized outside the glove box and dried at room temperature (approximately two weeks before analysis). The obtained powder was subsequently impregnated under high vacuum (800 Mbar) with an epoxy resin (Araldite® 502, Sigma-Aldrich). HA-Fe-As(V)*oxic* was synthesized from 20 mL of a 797 mg L^{-1} Leonardite suspension in which 1.4 mL of a 9.94 mg L^{-1} As(V) stock solution and 2 mL of a 1.38 g L^{-1} Fe(II) stock solution were added. The concentrations of DOC, Fe and As were 680.6, 117.8 and 0.60 mg L^{-1} respectively. The sample was dried at room temperature. Fh-As(III)*oxic* was prepared using the following procedure (Wilkie and Hering, 1996). A 0.1 M KOH stock solution was added dropwise with stirring to 500 mL of 0.05 mol L^{-1} $Fe(NO_3).9H_2O$. The pH reached a value of approximately 8 with the addition of 350 mL of 0.1 M KOH to ensure total Fe hydrolysis (Wilkie and Hering, 1996). A volume of 0.6 mL of a 0.05 M Na_2AsO_2 stock solution was added to obtain the desired concentration of 2 g L^{-1} and 11 mg L^{-1} for Fe and As respectively. The Fh-As(III)*oxic* suspension was aged for at least 24 hours with stirring. Then the suspension was washed three times with deionized water using centrifugation and dialyzed with 12-14 KDa cellulose membrane during 48 hours. The sample was dried at room temperature (approximately two weeks before analysis). Fh-

As(V)*oxic* was synthesized with the same protocol as Fh-As(III)*oxic*, using As(V) stock solution, with a target As/Fe ratio of 0.007. The lepidocrocite sample (Lp-As(V)*oxic*) was synthesized in the presence of As(V) according to the protocol given by Schwertmann and Cornell (1991) with an As/Fe mass ratio of 0.005 and was provided by A. Dia (Dia et al., 2015). The Lp-As(V)*oxic* was confirmed to be lepidocrocite using XRD analyses performed on a Siemens D500 diffractometer at the Chemical Sciences Department at the University of Rennes 1. Fh-As(III)*anoxic* was prepared by the adsorption of As(III) onto 2-line ferrihydrite synthesized according to Schwertmann and Cornell's protocol (1991) with an As/Fe ratio of 0.012. The As K-edge EXAFS spectra were provided by G. Ona-Nguema (Ona-Nguema et al., 2005). All of the obtained powders were pressed into 6 mm pellets for the Fe K-edge XAS analyses.

1.5 X-ray Absorption Spectroscopy (XAS)

1.5.1 Data collection

Arsenic K-edge spectra were collected on both the I18 beamline (Mosselmans et al., 2009) of the Diamond Light Source (DLS, Didcot, UK) and the 10.3.2 beamline (Marcus et al., 2004) of the Advanced Light Source (ALS, Berkeley, USA). Iron K-edge spectra were recorded on the LUCIA beamline (Flank et al., 2006) of the SOLEIL Synchrotron (SOLEIL, St Aubin, France). The monochromators used were Si(111) crystals. They were calibrated setting the first inflection point of the L-edge absorption spectrum of an Au foil to 11.918 KeV on I18, of a Na_2HAsO_4 standard to 11.875 KeV on 10.3.2 and of the K-edge of an Fe foil to 7.112 KeV on LUCIA. Spectra were collected in fluorescence mode using a 4-element Ge solid state detector on I18, a 7-element Ge solid state detector on 10.3.2 and a 4-element Silicon Drift Diode Detector on LUCIA. The beamsize on the sample was 2 x 3 µm on I18, 6 x 3 µm on 10.3.2 and 3 x 3 µm on LUCIA. To prevent beam-induced redox changes, samples were maintained under vacuum and at 70-80K using a liquid nitrogen cryostat on I18 and LUCIA. In the natural sample, prior to XAS acquisition, the spatial distribution of the elements in the sample was mapped by micro-X-ray fluorescence (µ-XRF). Based on the resulting maps, different types of spots were selected for the XAS analysis according to their As/Fe ratio as well as the As and Fe content. Fe K-edge XAS

reference spectra were collected with a beamsize set to 2 x 2 mm in transmission mode using a silicon diode for Fh-As(V)*oxic* and Lp-As(V)*oxic,* and in fluorescence mode for HA-Fe-As(III)*oxic*.

1.5.2 XAS data analysis

Arsenic and Fe XAS spectra were extracted using the Athena software (Ravel and Newville, 2005) including the Autbk algorithm (Rbkb = 1, k-weight = 3). Normalized spectra were obtained by fitting the pre-edge region with a linear function and the post-edge region with a quadratic polynomial function. The Fourier transform of the k^3-weighted EXAFS spectra were calculated over a range of 2-10.5 $Å^{-1}$ for As and 2-11 $Å^{-1}$ for Fe using an Hanning apodization window (window parameter = 1). Back Fourier filters were extracted over the 1.15-3.45 Å (1.15-3.85 Å for HA-Fe-As(III)*oxic*) and 1-3.8 Å R-range for As and Fe, respectively, using the same apodization window shape.

The relative proportions of As(III) and As(V) in the samples were determined by linear combination fitting (LCF) of the XANES spectra within the energy range of 11840-11940 eV using relevant As(III) and As(V) model compounds (i.e. As(III) and As(V) adsorbed onto ferrihydrite, the XANES white line position for As adsorbed on ferrihydrite being identical to that of As adsorbed on lepidocrocite (Ona-Nguema et al., 2005). The weighting factors were forced to be between 0 and 1 and the sum weights were not constrained in order to make sure that the references were suitable. All of the As(V) percents were recalculated to a component sum of 100%.

EXAFS data were analyzed by shell fitting using the software code Artemis (Ravel and Newville, 2005). Theoretical back scattering paths for the fits were calculated from different crystal structures using FEFF6. Scorodite (Kitahama et al., 1975) and tooeleite (Morin et al., 2007) structures were used to extract paths from backscatters of As(V) and As(III), respectively. Goethite (Hazemann et al., 1991), lepidocrocite (Zhukhlistov, 2001) and Fe-carboxylate (Horcajada et al., 2007) structures were used to obtain the backscattering paths for Fe. Shell-fit analyses were performed within the 1.15-3.5 Å and 1.15-3.85 Å R-range for As and 1-3.8 Å for Fe. The best fit was chosen by minimizing the reduced χ^2 which depends on the number of independent parameters, the number of fitted parameters and the uncertainty of the data points. For As, the addition of multiple scattering tends to improve the quality of the fit (Morin et al., 2002; Voegelin

et al., 2007). Here, the triangular As-O-O (MS1, degeneracy = 12), the collinear As-O-As-O (MS2 degeneracy = 4) and the non-collinear As-O-As-O (MS3, degeneracy = 12) paths were added for the fit of the $As^{(V)}O_4$-tetraedron. The MS1 path was constrained by an interatomic distance set to $(1 + (2/3)^{(1/2)}) \times R_{As\text{-}O}$ and a Debye-Waller parameter of $\sigma^2_{As\text{-}O}$. The MS2 path was constrained by an interatomic distance of $2R_{As\text{-}O}$ and its Debye-Waller parameter was calculated as $\sigma^2_{MS2} = 4 \times \sigma^2_{As-O}$. The interatomic distance of MS3 was defined as $2x\ R_{As\text{-}O}$ and its Debye-Waller parameter as $2 \times \sigma^2_{As-O}$ (Voegelin et al., 2007).

2 Results

2.1 Chemical analysis of the oxidation compound on the PTFE collector

The oxidation products collected on the PTFE scavengers were analyzed for major and trace elements. The concentrations obtained are given in Table 2 and compared with the soil horizon (A) and soil solution (SW). The origin in the soil solution of the oxidation products collected on the PTFE devices was previously determined by Al-Sid-Cheikh et al. (2015) following the rare earth element patterns of the soil solution and oxidation products. The Si and Al concentrations decreased from 30.4% and 30.0% in the soil to 1.1% and 0.5%, respectively, on the PTFE scavengers; which demonstrated the depletion of clay minerals and feldspars in the oxidation products compared to the soil organo mineral horizon. Conversely, the oxidation products were enriched in Fe and organic carbon (OC) with 8.5% of Fe and 75% of OC versus 1.1% of Fe, and 9% of OC in the soil. The As concentration increased from 7.39 mg Kg^{-1} in the soil to 239.31 mg Kg^{-1} on the PTFE scavenger surface. In the soil horizon and solution, the As/Fe ratio (wt/wt) was within the same order of magnitude, while this ratio increased by two orders of magnitude in the oxidation products. Thus, the oxidation products exhibited a strong enrichment in Fe, OC and furthermore in As.

2.2 NanoSIMS results

To investigate the distribution of As, the oxidation products were analyzed using a NanoSIMS probe. The ion distribution images for the $^{12}C^{14}N$, $^{56}Fe^{16}O$ and ^{75}As data are displayed in Figure 1. They highlight the heterogeneous distribution of the elements. The distribution of OM (as $^{12}C^{14}N$) and As (as ^{75}As) was

anticorrelated, while the As distribution followed that of Fe. Arsenic-enriched hotspots (i.e. red squares 1 and 2 in Figure 1) were also observed. The distribution of As thus followed two trends: i) it was diffused in the matrix and ii) concentrated in hotspots in which the colocalizations of the elements varied. In hotspot 1, high As counts were associated with high Fe and low OM counts whereas in hotspot 2, high As counts were associated with high OM and low Fe counts.

Pearson's coefficients (PC) were calculated to determine a statistic spatial distribution of the elements. However, using PCs alone may introduce ambiguity as PCs are highly dependent on signal intensity variations and on the heterogeneous colocalization relationships throughout the sample (Bolte and Cordelieres, 2006). Therefore, Mander's coefficients were calculated and taken into account when a positive colocalization was observed. The calculated Pearson's and Mander's statistic coefficients to determine the colocalizations in the entire image are displayed in Figure 2. The best correlation was observed for $^{56}Fe^{16}O/^{75}As$ with a PC value above 0.6 suggesting that the As distribution was intensively correlated to the one of Fe, as illustrated by hotspot 1. The determination of Manders' coefficients revealed that M1 and M2 were similar, thereby indicating that the As and Fe distributions were linked. When $^{56}Fe^{16}O$ was present, ^{75}As was also present in more than 60% of the cases and when ^{75}As was present, $^{56}Fe^{16}O$ was present in more than 65% of the cases. A positive Pearson's coefficient value close to 0.1 was calculated for $^{12}C^{14}N$ and ^{75}As indicating that there was no correlation in the entire image. However, a M2 value around 0.4 showed that a fraction of the ^{75}As pixels was associated with the $^{12}C^{14}N$ pixels; which was evidenced by hotspot 2.

2.3 Arsenic X-ray Absorption Spectroscopy

2.3.1 As oxidation state

The oxidation state of As in the natural sample was determined collecting the XANES spectra in 13 different spots and in the bulk. The spectra are reported in Figure 3 with the As(V) and As(III) synthesized references. The normalized spectra exhibit various shapes. Arsenic (III) bound to ferrihydrite under anoxic conditions and As (V) bound to ferrihydrite under oxic conditions were used as references for the As(III) and As(V) spectra, respectively, and for the LCF. They exhibited a white line maximum at 11871.2 eV and 11874.5 eV,

respectively. With regards to the synthesized samples of As(III) transferred into oxidizing conditions, As(III) associated with humic acid (HA-As(III)*oxic*) has a unique peak maximum at 11871.2 eV revealing no oxidation of As(III). In contrast, As(III) bound to ferrihydrite (Fh-As(III)*oxic*) exhibited a peak maximum at 11874.5 eV and did not show any shoulder at the low energy in the edge, suggesting that all of the As was entirely oxidized to As(V). The XANES spectrum of As(III) bound to Fe and HA (HA-Fe-As(III)*oxic*) exhibited two peaks at 11871.4 eV and 11874.8 eV, respectively, revealing the presence of both As(III) and As(V) with a proportion of 60% As(V) as determined by the LCF.

All of the natural sample spectra except two (i.e. Zone2-Spot1 and Zone1-Spot5) exhibited a shoulder at 11871.2 eV and a white line maximum at 11874.5 eV. The variations in intensity of the shoulder provide evidence of the presence of As(III) and As(V) at various proportions and heterogeneously distributed in the sample. The results of the LCF show that the As(V)/As(total) ratio ranged from 65% to 100%, depending on the studied spot. The bulk analysis showed 72% As(V), which corresponded to the average value of the measured ratios in the different spots. Both 100% As(V) spots (Zone2-Spot1 and Zone1-Spot5) exhibited features of a more crystallized structure revealed by the more pronounced oscillations in the post-edge region (Figure 3), possibly explained by a crystallized arsenate phase.

2.3.2 Nature and distance of the As neighbors

Despite the fact that our As concentration was rather low (i.e. 230 ppm in the digenetic precipitate) as compared to generally studied contaminated sites or As-enriched synthetic samples, it was possible to collect the EXAFS spectra in the bulk and in several spots. However, the low concentration explained the poorer signal/noise ratio quality compared to literature studies on samples artificially doped in As.

The As K-edge EXAFS data and the corresponding Fourier-Transform of the references and some spots collected in the natural sample are reported in Figure 4. Except for the HA-As(III)*oxic* reference, all of the EXAFS spectra exhibited a similar shape and oscillation positions. The second oscillation of the EXAFS spectra was characterized by a slight double-hump feature at approximately 6.7 and 7.4 $Å^{-1}$. The amplitude of the second hump was larger for the 100% As(V) spots and references, while the shoulder at 6.7 $Å^{-1}$ increased with the As(III) proportion. Additionally, the intensity of the oscillation at 8.3 $Å^{-1}$ decreased compared to the

one at 6.0 $Å^{-1}$ when a mixture of As(III)/As(V) occurred. The main peak in the Fourier transform was located at R + ΔR ~1.3 Å and corresponded to the first neighboring shell. The natural sample spots, bulk and references, except HA-As(III)*oxic*, exhibited one or two additional small peaks at R + ΔR ~2.3 Å and ~3.0 Å accounted for the second coordination shell neighbors. To explore the local coordination of As, fits were performed in the 1-3.5 Å R-range. The results are reported in Figure 4. The fitted parameters and constraints for the references and the natural sample bulk and spots are reported in Table 3.

***First Oxygen shell*.** All of the first coordination shells could be fitted with oxygen neighbors. With regards to the As(V) references, in Fh-As(V)*oxic* and HA-Fe-As(V)*oxic*, the number of O neighbors is close to 4 (3.9 and 4.1 respectively) at a distance of 1.70 Å. On the contrary, in the As(III) reference (i.e. Fh-As(III)*anoxic*), only 3.0 O were detected at a longer distance, 1.77 Å. These results are in accordance with previous studies on As(V) (Manning et al., 2002; Morin et al., 2008) and As(III) (Ona-Nguema et al., 2005; Thoral et al., 2005) adsorbed onto Fe(III)-oxyhydroxides. The reference materials submitted to an oxidation process, in HA-As(III)*oxic*, the XANES LCF showed no As(III) oxidation which was supported by the number and distance of the O neighbors, respectively 2.7, close to 3, and 1.76 Å. In contrast, As(III) coprecipitated with Fh (Fh-As(III)*oxic*), had 4.1 O at the same distance as Fh-As(V)*oxic*, 1.70 Å, confirming the XANES LCF calculation which revealed that all of the As(III) was fully oxidized to As(V). Because of the partial oxidation of As(III) into As(V) revealed by the XANES spectra for the HA-Fe-As(III)*oxic* reference as well as for the spots collected in the natural sample and for the bulk, in all of these samples, the first coordination shell fit gave intermediary results with 3.4 to 4.0 O at 1.70-1.71 Å. The number of calculated oxygen neighbors was in agreement with the As(V) content in the mixture of As(III) and As(V).

Second coordination shell. Except in HA-As(III)oxic, in which no path could be added to improve the fit performed with the oxygen backscattering path, two As-Fe distances were used to fit the second coordination shell. The longer one, referred to as the As-Fe_2 path, was included in all of the fits with 0.6 to 1.7 Fe at an As-Fe interatomic distance of 3.28-3.43 Å. These distances are in agreement with those reported for As(III) and As(V) monodentate binuclear corner-sharing complexes ^{2}C (Manceau, 1995; Ona-Nguema et al., 2005; Waychunas et al., 1993) where As(III) and/or As(V) were bound to the apical oxygen atoms of two

edge-sharing FeO_6 octahedra. The shorter distances (i.e. 3.28-3.33 Å) correspond to the references and samples that contain As(V) only, while the longer distances (i.e. (3.30)3.37-3.43 Å) correspond to the references and samples that contain As(III). These variations in the distances are in agreement with those reported by Farquhar et al. (2002) who additionally provided evidence of variations in the As-Fe distances as a function of the As-bearing Fe phase (namely As-Fe_2 distances are longer for As(III) binding to lepidocrocite than for As(III) binding to goethite). In the case of the references (Fh-As(III)*anoxic* and HA-Fe-As(III)*oxic*) and the natural samples containing enough As(III) (> 11%), a shorter As-Fe_1 path had to be added with 0.4 to 0.7 Fe at a distance of 2.82 to 2.95 Å. These Fe neighbor backscatterers are reported in the literature as being due to the formation of As(III) bidentate mononuclear edge-sharing complexes, ^{2}E (Manceau, 1995; Ona-Nguema et al., 2005; Waychunas et al., 1993). In spot 7, in which the As(III) concentration was low (i.e. 11%), this last As-Fe interatomic distance could not be added. Because our studied wetland was not enriched in As (close to 200 mg Kg^{-1} in the oxidation solids and only 7 mg Kg^{-1} in the soil) the data quality was surprisingly good considering the use of a microbeam for the XAS analysis.

2.4 Iron X-ray absorption spectroscopy

After µXRF elemental mapping of the natural sample, Fe K-edge XANES analyses were performed on six spots containing various levels of Fe enrichment in order to characterize the As carrier phases. All of the XANES spectra were fairly similar. The edge position at 7125 eV associated with a tiny pre-edge at 7114.2 eV and a broad shoulder at 7148 eV reflect octahedrally coordinated Fe(III) species in a poorly crystalline phase (data not shown). The EXAFS spectra and the corresponding Fourier transforms (magnitude and imaginary part) of the bulk and two spots along with the references (i.e. Fh-As(V)*oxic*, Lp-As(V)*oxic* and HA-Fe-As(III)*oxic*) are reported in Figure 5. The EXAFS spectra line shape of both the spots and bulk were similar. They were different from the references. Similarly to HA-Fe-As(III)*oxic* and in contrast to Fh-As(V)*oxic* and Lp-As(V)*oxic,* they did not exhibit any shoulder in the oscillation at 5.2 $Å^{-1}$. However, they exhibited a shoulder peak at 7.6 $Å^{-1}$, the intensity of which varied according to the spectrum. This peak existed in both Fe(III)-oxyhydroxides but shifted to the low k at 7.3 $Å^{-1}$. Two peaks dominated the Fourier transform of the natural sample and the references, except HA-Fe-As(III)*oxic*. The first peak, located at approximately 1.5 Å (R+ΔR), corresponded to

the first shell of the neighboring atoms within the FeO_6 octahedra. The second peak at approximatively 2.6 Å (R+ΔR) arose from the scattering of the Fe neighbors from the second coordination shell.

Shell fits were performed on the 1-3.8 A range of the Fourier transformed k^3-weighted spectra over a k-range 2-11 Å and displayed in Figure 5. The resulting EXAFS parameters of the fits are reported in Table 4.

First coordination shell. For the references and the natural sample, two Fe-O paths were required to accurately reproduce the first O shell, with Fe-O distances at 1.93-1.97 Å and 2.06-2.15 Å. These distances corresponded to the Fe-O distances for the octahedra in the Fe(III)-oxyhydroxides (Waychunas et al., 1993). The sum of the coordination numbers (N) of the Fe-O_1 and Fe-O_2 paths ranged from 4.3 to 6.7. Values lower than 6 ± 10% could be explained by partially destructive interferences for the individual scattering waves produced by the multiple Fe-O distances within the octahedron (Manceau and Gates, 1997; Voegelin et al., 2010).

Second coordination shell. The second peak at approximately 2.6 Å in the Fourier transforms (Figure 5) has a major contribution from the Fe neighbors. All of the spectra displayed a Fe-Fe_1 distance at 3.01-3.11 Å. This distance was characteristic of edge-sharing FeO_6 octahedra (Manceau and Combes, 1988; Manceau and Drits, 1993). The Fh-As(V)*oxic* and HA-Fe-As(III)*oxic* fit determined a Fe-Fe_2 distance at 3.44 and 3.49 Å respectively, specific to double corner-sharing as previously reported (Bottero et al., 1994; Manceau and Combes, 1988; Waychunas et al., 1993). The smaller number of Fe neighbors in HA-Fe-As(III)*oxic* than in Fh-As(V)*oxic* reflected the lower polymerization in the first reference. As in lepidocrocite, this distance did not exist in the natural sample spots and bulk while a longer Fe-Fe distance was determined at 3.84-4.02 Å, interpreted as a single corner-sharing octahedron, characteristic of a lepidocrocite structure (Manceau and Drits, 1993; Zhukhlistov, 2001). The absence of the 3.40 Å distance and the presence of the distance at approximately 3.90 Å in the natural sample, as in the lepidocrocite, therefore suggested that the Fe(III)-oxyhydroxides in the sample were lepidocrocite-like material. Lepidocrocite is commonly found in environments subject to oxic and anoxic fluctuations such as riparian wetlands (Schwertmann and Taylor, 1979). The coordination numbers for the Fe-Fe distances in the natural sample were much lower than in Lp-As(V)*oxic* suggesting the existence of nano-lepidocrocite in the natural sample. In HA-Fe-As(III)*oxic* as well as

in the bulk sample, the addition of an Fe-C path at 2.97 and 2.77 Å, respectively, improved the fit by 33% based on the R factor. To evaluate the relevance of adding Fe-C scattering path, we used a F-test adapted for EXAFS fitting by Downward et al. (2006). The results from the F-test demonstrated that the addition of an Fe-C path improved the fit at a confidence level of 89% which is higher than the required 67% (Downward et al., 2006). Karlsson and Persson (2010) obtained a similar Fe-C path in Fe bound to peat humic acid. They interpreted this result as the formation of small polynuclear Fe(III)-NOM complexes. The lack of the Fe-C distance in the natural sample spots could be explained by the fact that we have focused on Fe-enriched zones. The Fe-bearing phase appeared to be heterogeneous with nano-lepidocrocite hotspots and more diffuse Fe as small Fe-clusters bound to organic matter.

3 Discussion

Parameters controlling As(III) speciation

In the studied natural sample corresponding to the oxidation products of a riparian wetland solution As(III) was at least partially oxidized, with a As(V) proportion varying between 65 and 100% relative to the analyzed spots. These results were in agreement with previous observations in peatlands (ThomasArrigo et al., 2014), floodplains (Parsons et al., 2013) and paddy soils (Yamaguchi et al., 2014), which reported incomplete As(III) oxidation in oxidizing conditions.

Several studies have reported that the oxidation kinetics of As(III) by O_2 is slow in the natural environment (Lowry and Lowry, 2002; Thoral et al., 2005). In freshwater, Eary and Schramke (1990) reported a half-life ($t_{1/2}$) of several months to one year for As(III) oxidation by O_2. The XAS analysis performed on the synthesized references highlighted the notion that the presence of Fe(III)-oxyhydroxides drastically influenced the As oxidation process. In the Fh-As(III)*oxic* reference (without OM), the edge position together with the lack of an observable shoulder at low energy in the XANES spectrum and the number and distance of the oxygen neighbors showed a total oxidation of As(III) into As(V). This complete As(III) oxidation induced by the presence of Fe(III) have been previously reported by Greenleaf et al. (2003). Two mechanisms has been

proposed to explain the As(III) oxidation on the surface of the Fe(III)-oxyhydroxides. In the first hypothesis, dissolved O_2 was the oxidant of As(III) and the Fe(III)-oxyhydroxides acted as a catalyst (Auffan et al., 2008; Scott and Morgan, 1995; Zhao et al., 2011). This catalytic oxidation required an initial step of As(III) adsorption on Fe(III)-oxyhydroxides (Zhao et al., 2011). In the second hypothesis, Fe(III)-oxyhydroxides directly oxidized the adsorbed As(III) and released Fe(II) into the solution along with As(V). This latter species was possibly readsorbed onto the Fe(III)-oxyhydroxides (Greenleaf et al., 2003; Scott and Morgan, 1995). A portion of the Fe(II) is readsorbed onto the Fe(III)-oxyhydroxides (Greenleaf et al., 2003; Hiemstra and van Riemsdijk, 2007; Larese-Casanova and Scherer, 2007); however, Hiemstra and van Riemsdijk (2007) showed that at a pH below 7, as encountered in the studied wetland, readsorbed Fe remained as Fe(II). Note that no Fe(II) was detected from the XANES record at the Fe K-edge in any of our samples (references or natural sample) suggesting that the readsorption processes did not occur or were not significant. Finally, Ona-Nguema et al., 2005 demonstrated that lepidocrocite alone could not oxidize As(III). All of these arguments suggest that the Fe(III)-oxyhydroxide catalysis was the most likely prevailing mechanism for As(III) oxidation in the studied wetland, (i.e. dissolved O_2 was the oxidant of As(III) and the Fe(III)-oxyhydroxides acted as a catalyst).

The possibility of As(III) oxidation by autotrophic bacteria containing the aioA gene (Engel et al., 2013; Jiang et al., 2014; Sanyal et al., 2016) can be rejected. This is because with the large quantities of Fe(III)-oxyhydroxides present in our sample, that the oxidation of As(III) by such bacteria should be minor.

However, the persistence of As(III) in our natural sample suggested that an additional parameter influenced the As(III) oxidation process. Organic matter plays a significant role: addition of OM to the As(III)/Fe(III)-oxyhydroxide system tended to slow down the As(III) oxidation process, as shown by the LCF calculations on the XANES spectrum for the HA-Fe-As(III)*oxic* reference (with OM and Fe), which showed that 60% of As occurred as As(V). Furthermore, in the HA-As(III)*oxic* reference (without Fe), no oxidation of As(III) occurred, based on the edge shape and position in the XANES spectrum and the As-O distances at 1.76 Å (corresponding to the As(III)-O distance). The presence of OM in an As(III) solution stored under an oxidizing condition thus seemed to prevent As(III) oxidation or slow down the oxidation kinetics compared to the

reference material with Fe added. Two hypothesis can thus be considered: i) OM exerted a direct control on the reaction through As(III) binding onto its reduced surface groups, such as thiol (Catrouillet et al., 2014; Hoffmann et al., 2012; Langner et al., 2012); or ii) OM exerted an indirect control on the reaction by controlling the As binding phases.

The NanoSIMS analyses showed heterogeneity in the distribution of Fe, As and DOC. In addition to the diffused As in the sample matrix, As also appeared to be distributed in hotspots, mostly in Fe-enriched spots but also in several OM-enriched and Fe-depleted spots. Prior studies have provided evidence of the ability of OM to bind As via organosulfurs such as thiol groups (R-S-H) (Couture et al., 2013; Hoffmann et al., 2014; Langner et al., 2012). In a previous study on the same material as ours, a colocalization of As and S was observed by the nanoSIMS analysis (Al-Sid-Cheikh et al., 2015). The correlation of the As and OM distribution observed from the NanoSIMS images could be explained by the formation of such As-OM complexes. Despite the observed As-OM colocalization in some spots, the EXAFS data did not show evidence of the direct coordination of As with OM (no As-C or As-S distances) while the Fe neighbors were always present, even in the spots containing the highest proportion of As(III). These results could be explained by the different scales of investigation provided by each technique. NanoSims probes the nanoscale while µXAS probes the microscale. Because a maximum of 40% of As(III) was observed and if the formation of As-S-OM monodendate complexes were hypothesized (Catrouillet et al., 2014; Hoffmann et al., 2014), 12% of the first neighbors around As would be S, which is at the detection limit of the EXAFS measurements. Consequently, the EXAFS fitting of our samples did not show any S neighbors. Note that the studies in which As binding to OM via thiol was evidenced by EXAFS spectroscopy concern either thiol enriched synthetic samples (Hoffmann et al. 2014) or natural samples formed in strongly enriched As systems (Langner et al., 2012). Therefore, the hypothesis regarding a direct control of OM on As(III) oxidation could neither be confirmed or invalidated here.

The second hypothesis considered that OM exerted a control on the As carrier phases and thus had an indirect influence on the As(III) oxidation process. The EXAFS data collected at the Fe K-edge revealed a lepidocrocite structure (Manceau and Drits, 1993; Pinakidou et al., 2015; Zhukhlistov, 2001). In a peatland

area characterized by permanent flooding, ThomasArrigo et al. (2014) revealed that OM-enriched flocs contained both ferrihydrite and lepidocrocite. The difference in water saturation between peatlands and riparian wetlands is of major importance for the properties of OM and influences the formation process for Fe(III)-oxyhydroxides. Moreover, the formation of lepidocrocite (more crystallized than ferrihydrite) could be favored by several consecutive redox cycles as evidenced by Thompson et al. (2006) and shown by our samples. Yamaguchi et al. (2014), who studied As speciation in a paddy soil, observed under an oxic condition the persistence of As(III) associated with lepidocrocite in the outer rim of the roots and As(V) associated with goethite and ferrihydrite in the inner rim. They interpreted this difference as the result of a slow oxidation rate allowing the formation of lepidocrocite as compared to the permanent supply of O_2 by the root channel inducing a faster oxidation and the formation of goethite and ferrihydrite. The coordination numbers for the second coordination shell were much lower than for the lepidocrocite reference (Lp-As(V)*oxic*) revealing the nanometric size of the studied natural lepidocrocite. This low degree of polymerization could be explained by the high OM concentration (75%). In the field, at the beginning of the oxidation period (water level decrease), the DOC concentration could reach 38 mg L^{-1} (Table 2). Dissolved organic carbon, which is strongly heterogeneous and may be composed of various organic molecules such as humic substances, could impair crystal growth and the aggregation of Fe(III)-oxyhydroxides (Cornell and Schwertmann, 2003; Pédrot et al., 2011). Under the oxidation period, in the present OM-enriched wetland, As(III) was therefore mainly adsorbed onto nano-lepidocrocite, and As(III) oxidation should have been catalyzed by Fe. Auffan et al. (2008) suggested that not all of the binding sites were active during the catalysis of the As(III) oxidation by the Fe(III)-oxyhydroxides. They localized the active sites in a six-membered FeO_6 octahedral ring on the maghemite surface onto which As was bound as a ^2C corner-sharing complex. Ona-Nguema et al. (2005) reported that As(III) was bound onto particulate lepidocrocite only via ^2C corner-sharing complexes. However, in the present natural sample, the As-Fe interatomic distance detected, close to 2.8 Å, demonstrated the possibility that an ^2E edge-sharing complex between As(III) and the identified nano-lepidocrocite is formed. Ona-Nguema et al. (2005) explained this discrepancy with the results of Manning et al. (2002) and Farquhar et al. (2002) by differences in the surface coverage. The

number of ^{2}E sites in the lepidocrocite particles was limited compared to the ^{2}C sites. Therefore, when the surface coverage was higher, as in Ona-Nguema et al. (2005), ^{2}E would be masked by the increasing amount of ^{2}C. We calculated a concentration of 13.7 mg of As per g of Fe in Ona-Nguema et al. (2005) and 12 µg of As per g in Farquhar et al. (2002). This value is closer to the concentration of 2.81 µg of As per g of Fe in our study. The formation of nano-lepidocrocite leads to a different $^{2}C/^{2}E$ ratio value, compared to particulate lepidocrocite, with an increase in the ^{2}E edge-sharing sites compared to the ^{2}C corner-sharing sites. The Fe K-edge EXAFS analysis of the bulk indicated the existence of a Fe-C distance , suggesting to a lesser extent the presence of Fe(III) as monomers or Fe-polymers in the OM matrix. Karlsson and Persson (2010) suggested that this distance could be attributed to five-membered chelate rings between Fe and OM, but they did not determine the size of these structures. Mikutta and Kretzschmar (2011) and Hoffmann et al. (2013) suggested the presence of mononuclear Fe(III) species or small Fe(III) clusters depending on the Fe(III) concentration. In the natural sample, the only possibility for As(III) to be bound to these Fe(III) monomers or small clusters was as ^{2}E edge-sharing complexes. The formation of ^{2}C corner-sharing complexes of As on two adjacent Fe(III) monomers is impossible due to geometrical constraints. Therefore, ^{2}E complexes were favored with the formation of nano lepidocrocite and Fe(III) monomers. These hypotheses were supported by the variation in the coordination numbers for the ^{2}E and ^{2}C complexes between the bulk and the spots. In the spots, where the OM content varied compared to the bulk of the sample, the number of ^{2}E complexes increased whereas the ^{2}C complexes decreased. Arsenic(III) in ^{2}E edge-sharing complexes with nano-lepidocrocite and Fe monomers therefore helped to stabilize a fraction of As(III).

Involved mechanisms and environmental implication

In wetlands, under high water levels, when wetland soil saturation occurs, reducing conditions are developed. Soil and dissolved OM act as a source of C for Fe-reducing bacteria such as *Geobacter* (Dia et al., 2015). Subsequently, Fe(III)-oxyhydroxides are reductively dissolved and all of the associated elements (OM, metals, metalloids) are expected to be solubilized concomitantly. Under such high OM concentration conditions, OM prevents the formation of secondary Fe(II) minerals able to trap As by binding to Fe(II), and As is therefore maintained in solution mainly as labile species (Davranche et al., 2013; Catrouillet et al.,

2014). When the water level decreases and evapotranspiration increases, oxidized conditions are restored; Fe(II) is expected to aggregate first as amorphous Fe(III)-oxyhydroxides and then to evolve to nano-lepidocrocite stabilized by the high OM amount or is trapped as Fe(III) monomers or small clusters in the OM matrices. Such lepidocrocite stabilization has been previously observed by Chen et al., 2015. This oxidation/precipitation and trapping of Fe(III) probably first occurs through the formation of Fe/OM mixed colloids which, in a second time, progressively agglomerate and are deposited in the soil pores with the extent of the soil water disappearance. These associations are able to bind As(III). The size of the Fe phase results in a high capacity for As adsorption and thus an accumulation of As in the top level of the soil. In addition, the presence of OM partly prevents the oxidation of As(III) into As(V), thus preserving a certain quantity of the more toxic As species (i.e. As(III)) in the environment.

Based on this hypothesis, As mobility is entirely controlled by the transfer properties of their precursor colloidal form of the Fe/OM aggregates. This transfer ability is controlled by i) the size of the colloids, which controls their transport through the soil pores, as large colloids are rapidly eliminated with the water flow as shown in stormflow events (Neubauer et al., 2013) whereas small size colloids are retained for longer periods in the soil pores, ii) the soil porosity and permeability, and iii) the hydrophobicity and ionization capacity of the colloids, which controls their ability to be sorbed to the soil particles.

For a second time, after the aggregation and deposition of these Fe/OM associations in soil, As is immobilized with its carrying phase. In this situation, wetlands can be considered as retention or storage areas and not as the source of As as demonstrated by several authors, notably for the wetland and flooding plains along the Mekong (Fendorf, 2010; Kocar et al., 2008). However, the long term retention of As in riparian wetlands depends on the ability of such Fe/OM associations to persist in the wetland even under reducing conditions. Pédrot et al. (2011) demonstrated that Fe/OM associations are less stable with regards to bioreduction than the corresponding particulate Fe(III)-oxyhydroxides. However, Parsons et al. (2013) provided evidence that the repetitive redox cycle decreased As mobility and increased the As(V) proportion in the soil solid phase during the reduced half-cycle. They correlated this As(V) sequestration with the decreased dissolution of the Fe(III)-oxyhydroxides due to a finite DOC stock. In riparian wetlands, the supply

of OM is theoretically not limited but a poor quality of DOC (not enough metabolizable organic C) could have the same influence on the preservation of Fe(III)-oxyhydroxides in the system.

4 Conclusion

In this study we investigated the behavior of As and the role of OM during the reoxidation of a riparian wetland soil solution. PTFE scavengers were efficient devices to recover oxidation compounds directly from the soil.

The NanoSIMS results highlighted the heterogeneous repartitioning of As, Fe and OM within the sample as well as different colocalizations between the elements. A strong correlation existed between Fe and As distribution but several As and OM-enriched hotspots depleted in Fe were also observed. The assumption that these hotspots revealed direct binding between As and OM via the thiol groups was made, however we were not able to confirm this direct control by OM on As speciation using the XAS measurements. In our study, As was adsorbed onto Fe(III)-oxyhydroxides as As(III) and As(V). The presence of As(III) under such oxidizing conditions was explained by a partial oxidation of As(III) indirectly controlled by the presence of high quantities of OM. First, the presence of a large amount of OM in our wetland results in the formation of i) nano-lepidocrocite with a high specific surface area and of ii) small-Fe clusters bound to OM. The formation of both structures promoted As binding as ^{2}E complexes which are not able to oxidize As(III) (compared to ^{2}C corner-sharing complexes). This process resulted in the retention of a significant proportion of As(III) in the samples , even under oxidizing conditions.

In our studied riparian wetland, the soil seems to act as a retention area for As and not as the source of As, as already proposed by several authors.

Acknowledgements

We acknowledge the Advanced Light Source, the Diamond Light Source and SOLEIL synchrotron for provision of synchrotron radiation facilities and we would like to thank the beamlines staff for their support, especially S. Fakra for her assistance on the 10.3.2 beamline and T.Geraki for her assistance on the I18 beamline. The Advanced Light Source is supported by the Director, Office of Science, Office of Basic Energy Sciences, of the

U.S. Department of Energy under Contract No. DE-AC02-05CH11231. Many thanks to G. Ona-Nguema for fruitful discussion and kindly providing us with the Fh-As(III)*anoxic* spectra. We also thank Martine Bouhnik-Le Coz and Xavier Le Coz for their assistance for chemical analysis and sample preparation. Dr. S. Mullin is acknowledged for post-editing the English style (http://www.proz.com/profile/677614).

This study was funded by the French ANR through the "Programme Jeunes Chercheurs" (ANR-JC-11-JS56-0010, ARSENORG) and by the IUF (Institut Universitaire de France) allocation of Melanie Davranche.

5 Bibliography

Al-Sid-Cheikh, M., Pédrot, M., Dia, A., Guenet, H., Vantelon, D., Davranche, M., Gruau, G., Delhaye, T., 2015. Interactions between natural organic matter, sulfur, arsenic and iron oxides in re-oxidation compounds within riparian wetlands: NanoSIMS and X-ray adsorption spectroscopy evidences. Sci. Total Environ. 515-516, 118–128. doi:10.1016/j.scitotenv.2015.02.047

Auffan, M., Rose, J., Proux, O., Borschneck, D., Masion, A., Chaurand, P., Hazemann, J.-L., Chaneac, C., Jolivet, J.-P., Wiesner, M.R., Van Geen, A., Bottero, J.-Y., 2008. Enhanced Adsorption of Arsenic onto Maghemites Nanoparticles: As(III) as a Probe of the Surface Structure and Heterogeneity. Langmuir 24, 3215–3222. doi:10.1021/la702998x

Belzile, N., De Vitre, R.R., Tessier, A., 1989. In situ collection of diagenetic iron and manganese oxyhydroxdes from natural sediments. Nature 340, 376–377.

Bolte, S., Cordelieres, F.P., 2006. A guided tour into subcellular colocalization analysis in light microscopy. J. Microsc. 224, 213–232.

Bottero, J.Y., Manceau, A., Villieras, F., Tchoubar, D., 1994. Structure and mechanisms of formation of FeOOH(Cl) polymers. Langmuir 10.

Bourrié, G., Trolard, F., Jaffrezic, J.-M.R.G., Maître, V., Abdelmoula, M., 1999. Iron control by equilibria between hydroxy-green rusts and solutions in hydromorphic soils. Geochim. Cosmochim. Acta 63, 3417–3427.

Catrouillet, C., Davranche, M., Dia, A., Bouhnik-Le Coz, M., Marsac, R., Pourret, O., Gruau, G., 2014. Geochemical modeling of Fe(II) binding to humic and fulvic acids. Chem. Geol. 372, 109–118. doi:10.1016/j.chemgeo.2014.02.019

Catrouillet, C., Davranche, M., Dia, A., Bouhnik-Le Coz, M., Pédrot, M., Marsac, R., Gruau, G., 2015. Thiol groups controls on arsenite binding by organic matter: New experimental and modeling evidence. J. Colloid Interface Sci. 460, 310–320. doi:10.1016/j.jcis.2015.08.045

Chen, C., Kukkadapu, R., Sparks, D.L., 2015. Influence of Coprecipitated Organic Matter on $Fe^{2+}_{(aq)}$ -Catalyzed Transformation of Ferrihydrite: Implications for Carbon Dynamics. Environ. Sci. Technol. 49, 10927–10936. doi:10.1021/acs.est.5b02448

Combes, J.M., Manceau, A., Calas, G., Bottero, J.Y., 1989. Formation of ferric oxides from aqueous solutions: A polyhedral approach by X-ray absorption spectroscopy: 1. Hydrolysis and formation of ferric gels. Geochim. Cosmochim. Acta 53, 583–594.

Cornell, R.M., Schwertmann, U., 2003. The Iron Oxides: Structures, Properties, Reactions, Occurence and Uses, VCH. ed. Weinheim, Germany.

Couture, R.-M., Wallschläger, D., Rose, J., Van Cappellen, P., 2013. Arsenic binding to organic and inorganic sulfur species during microbial sulfate reduction: a sediment flow-through reactor experiment. Environ. Chem. 10, 285. doi:10.1071/EN13010

Davranche, M., Dia, A., Fakih, M., Nowack, B., Gruau, G., Ona-nguema, G., Petitjean, P., Martin, S., Hochreutener, R., 2013. Organic matter control on the reactivity of Fe(III)-oxyhydroxides and associated As in wetland soils: A kinetic modeling study. Chem. Geol. 335, 24–35. doi:10.1016/j.chemgeo.2012.10.040

Davranche, M., Grybos, M., Gruau, G., Pédrot, M., Dia, A., Marsac, R., 2011. Rare earth element patterns: A tool for identifying trace metal sources during wetland soil reduction. Chem. Geol. 284, 127–137. doi:10.1016/j.chemgeo.2011.02.014

Dia, A., Gruau, G., Olivié-Lauquet, G., Riou, C., Molénat, J., Curmi, P., 2000. The distribution of rare earth elements in groundwaters: assessing the role of source-rock composition, redox changes and colloidal particles. Geochim. Cosmochim. Acta 64, 4131–4151.

Dia, A., Lauga, B., Davranche, M., Fahy, A., Duran, R., Nowack, B., Petitjean, P., Henin, O., Martin, S., Marsac, R., Gruau, G., 2015. Bacteria-mediated reduction of As(V)-doped lepidocrocite in a flooded soil sample. Chem. Geol. 406, 34–44. doi:10.1016/j.chemgeo.2015.04.008

Downward, L., Booth, C.H., Lukens, W.W., Bridges, F., 2006. A variation of the F-test for determining statistical relevance of particular parameters in EXAFS fits. Lawrence Berkeley Natl. Lab.

Engel, A.S., Johnson, L.R., Porter, M.L., 2013. Arsenite oxidase gene diversity among *C hloroflexi* and *P roteobacteria* from El Tatio Geyser Field, Chile. FEMS Microbiol. Ecol. 83, 745–756. doi:10.1111/1574-6941.12030

Farquhar, M.L., Charnock, J.M., Livens, F.R., Vaughan, D.J., 2002. Mechanisms of Arsenic Uptake from Aqueous Solution by Interaction with Goethite, Lepidocrocite, Mackinawite, and Pyrite: An X-ray Absorption Spectroscopy Study. Environ. Sci. Technol. 36, 1757–1762. doi:10.1021/es010216g

Fendorf, S., 2010. Arsenic chemistry in soils and sediments. Lawrence Berkeley Natl. Lab.

Flank, A.-M., Cauchon, G., Lagarde, P., Bac, S., Janousch, M., Wetter, R., Dubuisson, J.-M., Idir, M., Langlois, F., Moreno, T., Vantelon, D., 2006. LUCIA, a microfocus soft XAS beamline. Nucl. Instrum. Methods Phys. Res. Sect. B Beam Interact. Mater. At. 246, 269–274. doi:10.1016/j.nimb.2005.12.007

Greenleaf, J.E., Cumbal, L., Staina, I., Sengupta, A.K., 2003. Abiotic As(III) oxidation by hydrated Fe(III) oxide (HFO) microparticles in a plug flow columnar configuration. Process Saf. Environ. Prot. 81, 87–98.

Gruau, G., Dia, A., Olivié-Lauquet, G., Davranche, M., Pinay, G., 2004. Controls on the distribution of rare earth elements in shallow groundwaters. Water Res. 38, 3576–3586. doi:10.1016/j.watres.2004.04.056

Grybos, M., Davranche, M., Gruau, G., Petitjean, P., 2007. Is trace metal release in wetland soils controlled by organic matter mobility or Fe-oxyhydroxides reduction? J. Colloid Interface Sci. 314, 490–501. doi:10.1016/j.jcis.2007.04.062

Grybos, M., Davranche, M., Gruau, G., Petitjean, P., Pédrot, M., 2009. Increasing pH drives organic matter solubilization from wetland soils under reducing conditions. Geoderma 154, 13–19. doi:10.1016/j.geoderma.2009.09.001

Hazemann, J.-L., Bérar, J.F., Manceau, A., 1991. Rietveld Studies of the Aluminium-Iron Substitution in Synthetic Goethite. Mater. Sci. Forum 79-82, 821–826.

Hiemstra, T., van Riemsdijk, W.H., 2007. Adsorption and surface oxidation of Fe(II) on metal (hydr)oxides. Geochim. Cosmochim. Acta 71, 5913–5933. doi:10.1016/j.gca.2007.09.030

Hoffmann, M., Mikutta, C., Kretzschmar, R., 2014. Arsenite binding to sulfhydryl groups in the absence and presence of ferrihydrite: a model study. Environ. Sci. Technol. 48, 3822–3831.

Hoffmann, M., Mikutta, C., Kretzschmar, R., 2013. Arsenite Binding to Natural Organic Matter: Spectroscopic Evidence for Ligand Exchange and Ternary Complex Formation. Environ. Sci. Technol. 47, 12165–12173. doi:10.1021/es4023317

Hoffmann, M., Mikutta, C., Kretzschmar, R., 2012. Bisulfide Reaction with Natural Organic Matter Enhances Arsenite Sorption: Insights from X-ray Absorption Spectroscopy. Environ. Sci. Technol. 46, 11788–11797. doi:10.1021/es302590x

Horcajada, P., Surble, S., Serre, C., Hong, D.-Y., Seo, Y.K., Chang, J.S., Greneche, J.M., Margiolaki, I., Ferey, G., 2007. Synthesis and catalytic properties of MIL-100(Fe), an iron(iii) carboxylate with large pores. Chem. Commun. 2820. doi:10.1039/b704325b

Jiang, Z., Li, P., Jiang, D., Wu, G., Dong, H., Wang, Y., Li, B., Wang, Y., Guo, Q., 2014. Diversity and abundance of the arsenite oxidase gene aioA in geothermal areas of Tengchong, Yunnan, China. Extremophiles 18, 161–170. doi:10.1007/s00792-013-0608-7

Karlsson, T., Persson, P., 2010. Coordination chemistry and hydrolysis of Fe(III) in a peat humic acid studied by X-ray absorption spectroscopy. Geochim. Cosmochim. Acta 74, 30–40. doi:10.1016/j.gca.2009.09.023

Kitahama, K., Kiriyama, R., Baba, Y., 1975. Refinement of crystal-structure of scorodite. Acta Crystallogr. Sect. B-Struct. Sci. 31, 322–324.

Kocar, B.D., Polizzotto, M.L., Benner, S.G., Ying, S.C., Ung, M., Ouch, K., Samreth, S., Suy, B., Phan, K., Sampson, M., Fendorf, S., 2008. Integrated biogeochemical and hydrologic processes driving arsenic release from shallow sediments to groundwaters of the Mekong delta. Appl. Geochem. 23, 3059–3071. doi:10.1016/j.apgeochem.2008.06.026

Langner, P., Mikutta, C., Kretzschmar, R., 2012. Arsenic sequestration by organic sulphur in peat. Nat. Geosci. 5, 66–73. doi:10.1038/ngeo1329

Larese-Casanova, P., Scherer, M.M., 2007. Fe (II) sorption on hematite: New insights based on spectroscopic measurements. Environ. Sci. Technol. 41, 471–477.

Lowry, J.D., Lowry, S.B., 2002. Oxidation of As(III) by aeration and storage. NRML Off. Res. Dev.

Manceau, A., 1995. The mechanism of anion adsortion on iron oxides: Evidence for the bonding of arsenate tetrahedra on free Fe(O,OH)6 edges. Geochim. Cosmochim. Acta 59, 3647–3653.

Manceau, A., Combes, J.M., 1988. Structure of Mn and Fe oxides and oxyhydroxides: a topological approach by EXAFS. Phys. Chem. Miner. 15, 283–295.

Manceau, A., Drits, V.A., 1993. Local structure of ferrihydrite and feroxyhite by EXAFS spectroscopy. Clay Miner. 28, 165–184.

Manceau, A., Gates, W.P., 1997. Surface structural model for ferrihydrite. Clays Clay Miner. 45, 448–460.

Manders, E.M.M., Verbeek, F.J., Aten, J.A., 1993. Measurement of co-localization of objects in dual-colour confocal images. J. Microsc. 169, 375–382.

Manning, B.A., Hunt, M.L., Amrhein, C., Yarmoff, J.A., 2002. Arsenic (III) and arsenic (V) reactions with zerovalent iron corrosion products. Environ. Sci. Technol. 36, 5455–5461.

Marcus, M.A., MacDowell, A.A., Celestre, R., Manceau, A., Miller, T., Padmore, H.A., Sublett, R.E., 2004. Beamline 10.3.2 at ALS: a hard X-ray microprobe for environmental and materials sciences. J. Synchrotron Radiat. 11, 239–247.

Mikutta, C., Kretzschmar, R., 2011. Spectroscopic Evidence for Ternary Complex Formation between Arsenate and Ferric Iron Complexes of Humic Substances. Environ. Sci. Technol. 45, 9550–9557. doi:10.1021/es202300w

Morin, G., Lecocq, D., Juillot, F., Calas, G., Ildefonse, P., Belin, S., Briois, V., Dillmann, P., Chevallier, P., Gauthier, C., others, 2002. EXAFS evidence of sorbed arsenic (V) and pharmacosiderite in a soil overlying the Echassières geochemical anomaly, Allier, France. Bull. Société Géologique Fr. 173, 281–291.

Morin, G., Ona-Nguema, G., Wang, Y., Menguy, N., Juillot, F., Proux, O., Guyot, F., Calas, G., Brown Jr., G.E., 2008. Extended X-ray Absorption Fine Structure Analysis of Arsenite and Arsenate Adsorption on Maghemite. Environ. Sci. Technol. 42, 2361–2366. doi:10.1021/es072057s

Morin, G., Rousse, G., Elkaim, E., 2007. Crystal structure of tooeleite, Fe6(AsO3)4SO4(OH)4{middle dot}4H2O, a new iron arsenite oxyhydroxy-sulfate mineral relevant to acid mine drainage. Am. Mineral. 92, 193–197. doi:10.2138/am.2007.2361

Mosselmans, J.F.W., Quinn, P.., Dent, A.J., Cavill, S.., Moreno, S.D., 2009. I18-the microfocus spectroscopy beamline at the Diamond Light Source. J. Synchrotron Radiat. 16, 818–824.

Neubauer, E., Köhler, S.J., von der Kammer, F., Laudon, H., Hofmann, T., 2013. Effect of pH and Stream Order on Iron and Arsenic Speciation in Boreal Catchments. Environ. Sci. Technol. 47, 7120–7128. doi:10.1021/es401193j

Olivié-Lauquet, G., Gruau, G., Dia, A., Riou, C., Jaffrezic, A., Henin, O., 2001. Release of trace elements in wetlands: role of seasonal variability. Water Res. 35, 943–952.

Ona-Nguema, G., Morin, G., Juillot, F., Calas, G., Brown, G.E., 2005. EXAFS Analysis of Arsenite Adsorption onto Two-Line Ferrihydrite, Hematite, Goethite, and Lepidocrocite. Environ. Sci. Technol. 39, 9147–9155. doi:10.1021/es050889p

Parsons, C.T., Couture, R.-M., Omoregie, E.O., Bardelli, F., Greneche, J.-M., Roman-Ross, G., Charlet, L., 2013. The impact of oscillating redox conditions: Arsenic immobilisation in contaminated calcareous floodplain soils. Environ. Pollut. 178, 254–263. doi:10.1016/j.envpol.2013.02.028

Pédrot, M., Boudec, A.L., Davranche, M., Dia, A., Henin, O., 2011a. How does organic matter constrain the nature, size and availability of Fe nanoparticles for biological reduction? J. Colloid Interface Sci. 359, 75–85. doi:10.1016/j.jcis.2011.03.067

Pédrot, M., Boudec, A.L., Davranche, M., Dia, A., Henin, O., 2011b. How does organic matter constrain the nature, size and availability of Fe nanoparticles for biological reduction? J. Colloid Interface Sci. 359, 75–85. doi:10.1016/j.jcis.2011.03.067

Pédrot, M., Dia, A., Davranche, M., Bouhnik-Le Coz, M., Henin, O., Gruau, G., 2008. Insights into colloid-mediated trace element release at the soil/water interface. J. Colloid Interface Sci. 325, 187–197. doi:10.1016/j.jcis.2008.05.019

Pinakidou, F., Katsikini, M., Simeonidis, K., Paloura, E.C., Mitrakas, M., 2015. An X-ray absorption study of synthesis- and As adsorption-induced microstructural modifications in Fe oxy-hydroxides. J. Hazard. Mater. 298, 203–209. doi:10.1016/j.jhazmat.2015.05.037

Polizzotto, M.L., Kocar, B.D., Benner, S.G., Sampson, M., Fendorf, S., 2008. Near-surface wetland sediments as a source of arsenic release to ground water in Asia. Nature 454, 505–508. doi:10.1038/nature07093

Ravel, B., Newville, M., 2005. ATHENA, ARTEMIS, HEPHAESTUS: data analysis for X-ray absorption spectroscopy using IFEFFIT. J. Synchrotron Radiat. 12, 537–541. doi:10.1107/S0909049505012719

Sanyal, S.K., Mou, T.J., Chakrabarty, R.P., Hoque, S., Hossain, M.A., Sultana, M., 2016. Diversity of arsenite oxidase gene and arsenotrophic bacteria in arsenic affected Bangladesh soils. AMB Express 6. doi:10.1186/s13568-016-0193-0

Schwertmann, U., Cornell, R.M., 1991. Iron oxides in the Laboratory: Preparation and Characterization, Wiley-VCH. ed. Weinheim, Germany.

Schwertmann, U., Taylor, R.M., 1979. Natural and synthetic poorly crystallized lepidocrocite. Clay Miner. 14, 285–293.

Scott, M.J., Morgan, J.J., 1995. Reactions at oxide surfaces. 1. Oxidation of As (III) by synthetic birnessite. Environ. Sci. Technol. 29, 1898–1905.

Tang, J., Johannesson, K.H., 2003. Speciation of rare earth elements in natural terrestrial waters: assessing the role of dissolved organic matter from the modeling approach. Geochim. Cosmochim. Acta 67, 2321–2339. doi:10.1016/S0016-7037(02)01413-8

Teasdale, P.R., Allen, L., Apte, S.C., Batley, G.E., Birch, G., 1998. In situ collection of diagenetic and induced oxyhydroxide precipitates from riverine and estuarine sediments. Environ. Technol. 19, 1191–1201.

ThomasArrigo, L.K., Mikutta, C., Byrne, J., Barmettler, K., Kappler, A., Kretzschmar, R., 2014. Iron and Arsenic Speciation and Distribution in Organic Flocs from Streambeds of an Arsenic-Enriched Peatland. Environ. Sci. Technol. 48, 13218–13228. doi:10.1021/es503550g

Thompson, A., Chadwick, O.A., Rancourt, D.G., Chorover, J., 2006. Iron-oxide crystallinity increases during soil redox oscillations. Geochim. Cosmochim. Acta 70, 1710–1727. doi:10.1016/j.gca.2005.12.005

Thoral, S., Rose, J., Garnier, J.M., Van Geen, A., Refait, P., Traverse, A., Fonda, E., Nahon, D., Bottero, J.Y., 2005. XAS study of iron and arsenic speciation during Fe (II) oxidation in the presence of As (III). Environ. Sci. Technol. 39, 9478–9485.

Voegelin, A., Kaegi, R., Frommer, J., Vantelon, D., Hug, S.J., 2010. Effect of phosphate, silicate, and Ca on Fe(III)-precipitates formed in aerated Fe(II)- and As(III)-containing water studied by X-ray absorption spectroscopy. Geochim. Cosmochim. Acta 74, 164–186. doi:10.1016/j.gca.2009.09.020

Voegelin, A., Weber, F.-A., Kretzschmar, R., 2007. Distribution and speciation of arsenic around roots in a contaminated riparian floodplain soil: Micro-XRF element mapping and EXAFS spectroscopy. Geochim. Cosmochim. Acta 71, 5804–5820. doi:10.1016/j.gca.2007.05.030

Waychunas, G.A., Rea, B.A., Fuller, C.C., Davis, J.A., 1993. Surface chemistry of ferrihydrite: Part1. EXAFS studies of the geometry of coprecipitated and adsorbed arsenate. Geochim. Cosmochim. Acta 57, 2251–2269.

Wilkie, J.A., Hering, J.G., 1996. Adsorption of arsenic onto hydrous ferric oxide: effects of adsorbate/adsorbent ratios and co-occurring solutes. Colloids Surf. -Physicochem. Eng. Asp. 107, 97–110.

Yamaguchi, N., Ohkura, T., Takahashi, Y., Maejima, Y., Arao, T., 2014. Arsenic Distribution and Speciation near Rice Roots Influenced by Iron Plaques and Redox Conditions of the Soil Matrix. Environ. Sci. Technol. 48, 1549–1556. doi:10.1021/es402739a

Zhao, Z., Jia, Y., Xu, L., Zhao, S., 2011. Adsorption and heterogeneous oxidation of As(III) on ferrihydrite. Water Res. 45, 6496–6504. doi:10.1016/j.watres.2011.09.051

Zhukhlistov, A.P., 2001. Crystal structure of lepidocrocite FeO (OH) from the electron-diffractometry data. Crystallogr. Rep. 46, 730–733.

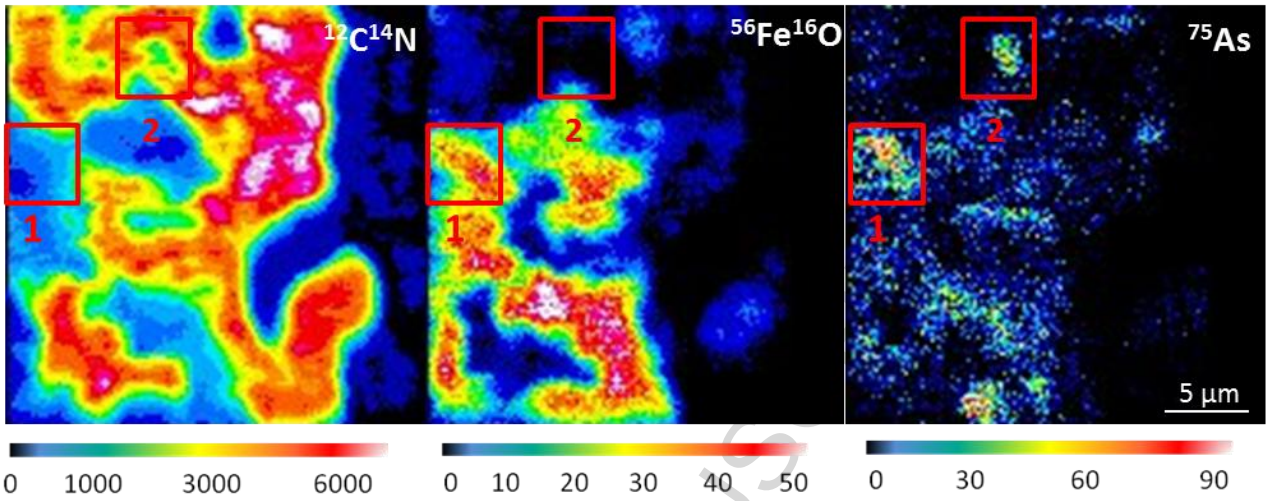

Figure 1 NanoSIMS images of the distribution of organic matter ($^{12}C^{14}N$), iron ($^{56}Fe^{16}O$) and arsenic (^{75}As) in the oxidation products. The red squares correspond to two As hotspots.

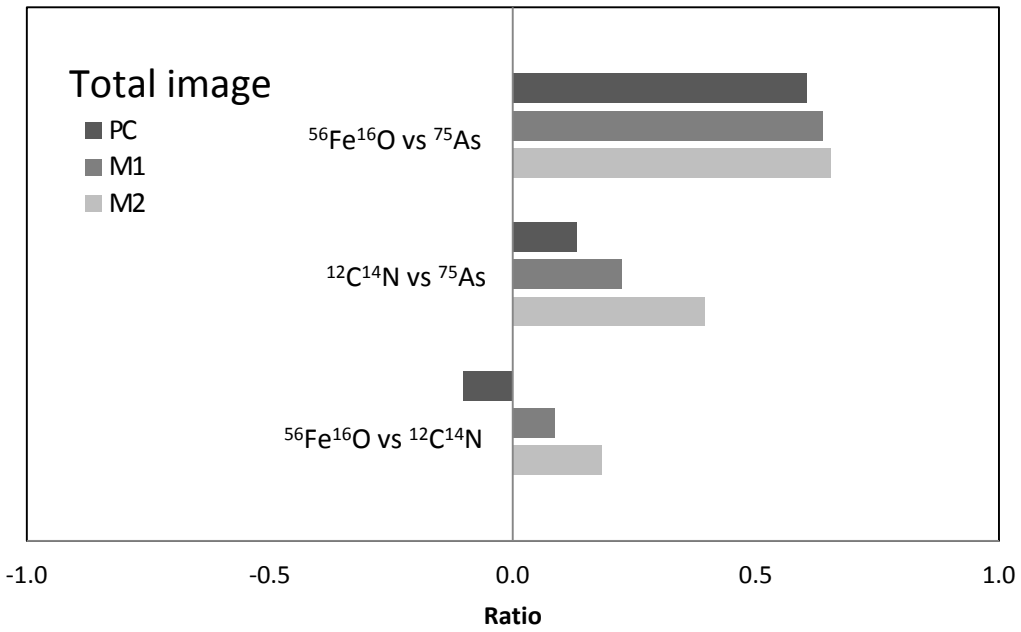

Figure 2 Colocalization of $^{56}Fe^{16}O$, ^{75}As and $^{12}C^{14}N$ using Pearson's (PC) and Manders' (M1 and M2) coefficients within the entire image

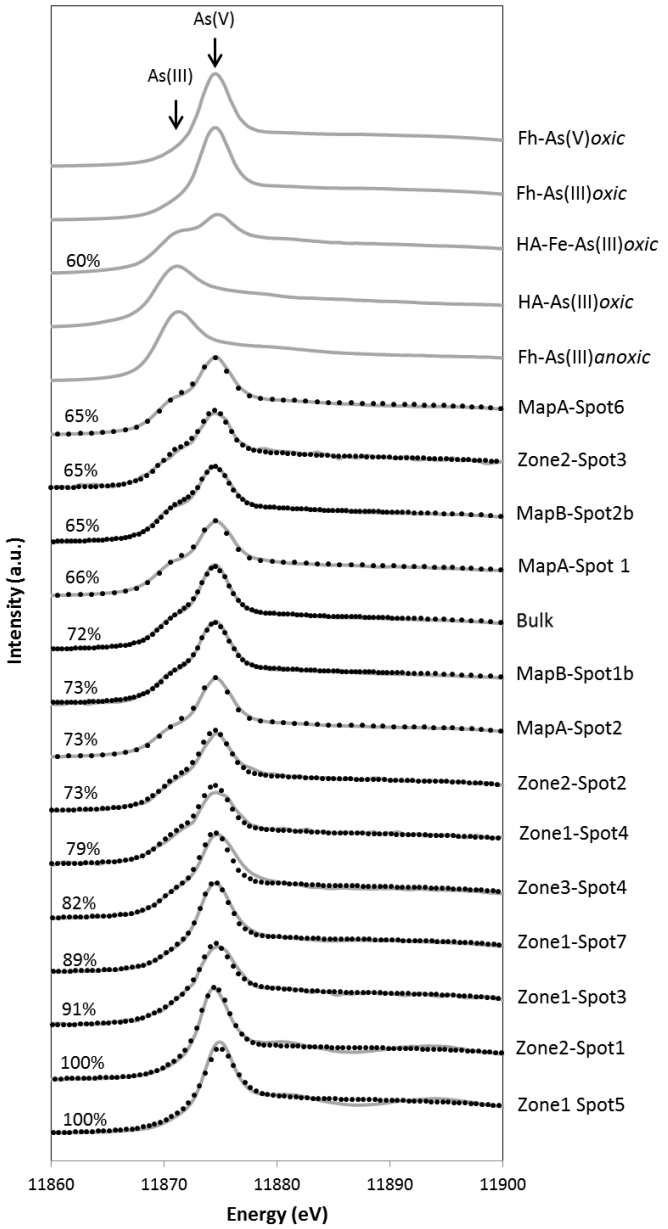

Figure 3 As K-edge X-ray absorption near-edge structure (XANES) spectra for different spots and the bulk of the natural sample along with the references. Solid lines correspond to experimental data and dashed lines are the linear combination fitting results. The calculation of the As(III) and As(V) contribution (expressed with As(V) percentage) to the natural sample derived from the LCF results are shown above each spectrum.

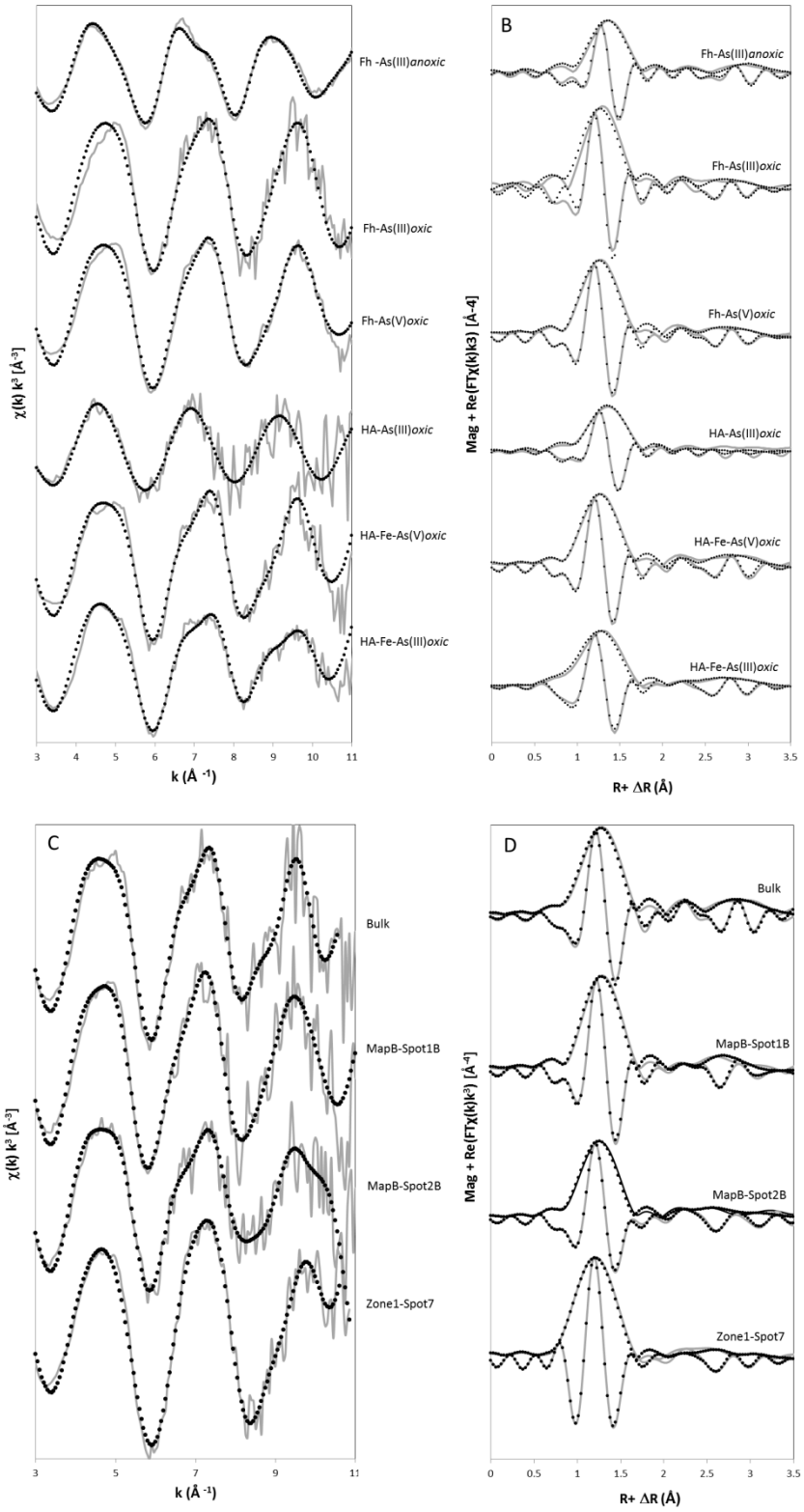

Figure 4 Arsenic K-edge EXAFS spectra and magnitude and imaginary part of the Fourier transform (uncorrected from the phase shift) of references A) and B) respectively, and of the natural sample bulk and three spots, C) and D) respectively. The fit results, given as dotted lines, are superimposed onto the data in solid grey lines.

1

1 .

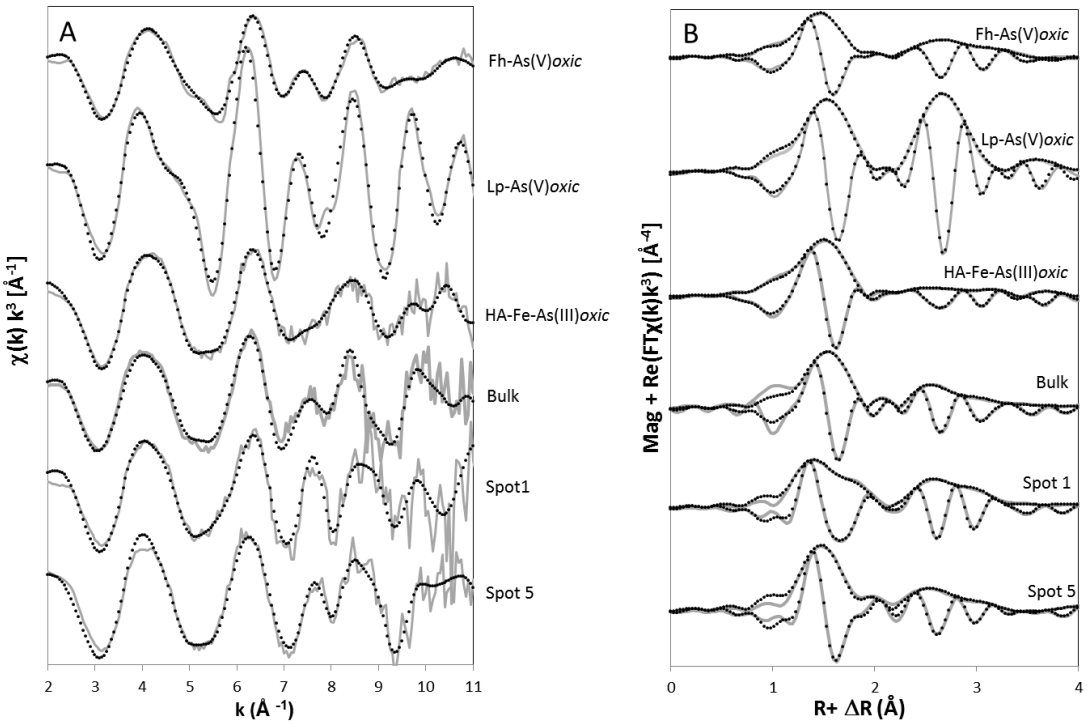

2
3 **Figure 5** A) Iron K-edge EXAFS spectra of the references and two spots and the bulk of the naturel sample and synthetic references
4 (Fh: ferrihydrite, Lp: lepidocrocite) and B) magnitude and imaginary part of the associated Fourier transform (uncorrected for the
5 phase shift). Solid lines are experimental data and dotted lines are the fit results.

6
7

1 **Table 1** References used for XAS analysis at the As and Fe K-edge

Sample	Binding method	As/Fe ratio	As/DOC ratio	Reference
As K-edge references				
Fh-As(III)*anoxic*	adsorption	0.012	-	(a)
Fh-As(III)*oxic*	coprecipitation	0.005	-	this study
Fh-As(V)*oxic*	coprecipitation	0.007	-	this study
HA-As(III)*oxic*	coprecipitation	-	$8.5\ 10^{-4}$	this study
HA-Fe-As(V)*oxic*	coprecipitation	0.005	$8.8\ 10^{-4}$	this study
HA-Fe-As(III)*oxic*	coprecipitation	0.004	$8.7\ 10^{-4}$	this study
Fe K-edge references				
Fh-As(V)*oxic*	coprecipitation	0.007	-	this study
Lp-As(V)*oxic*	coprecipitation	0.005	-	(b)
HA-Fe-As(III)*oxic*	coprecipitation	0.004	$8.7\ 10^{-4}$	this study

2
3 (a) Ona-Nguema et al, 2005
4 (b) Dia et al, 2015
5
6

Table 2 Major elements and As content of a wetland soil sample, surface water and oxidation products precipitated on PTFE scavengers

	Si	Al	Fe	K	Mg	Na	Ca	OC	As
	%								mg.Kg-1
A[a]	30.4	30.0	1.1	0.8	0.3	0.1	0.2	9	7.4
PTFE scavenger[b]	1.1	0.5	8.5	0.1	0.2	0.1	0.6	75	239.3
	mg.Kg-1								
SW[c]	4.49	0.28	1.29	0.77	10.83	13.41	6.01	38.0	5.5E-04

a: Organo-mineral horizon (0-15 cm)
b: Oxidation compounds precipitate on the PTFE scavengers
c: Surface water

Table 3 Shell-Fit parameters determined from the As K-edge EXAFS spectra of four spots and the bulk of the natural sample compared to the references

		As-O			As-Fe1			As-Fe2				
Sample	% As(V)	R[a]	N[b]	σ^{2} [c]	R	N	σ^{2}	R	N	σ^{2}	ΔE(eV)[d]	R factor[e]
Fh-As(III) *anoxic*	0	1.77 ± 0.01	3.0 ± 0.3	0.003	2.88 ± 0.04	0.7 ± 0.4	0.007	3.37 ± 0.04	1.0 ± 0.7	0.007	9.0 ± 0.7	0.015
Fh-As(III) *oxic*	100	1.70 ± 0.01	4.1 ± 0.3	0.002				3.31 ± 0.05	1.3 ± 0.9	0.007	9.6 ± 0.7	0.030
Fh-As(V) *oxic*	100	1.70 ± 0.01	4.1 ± 0.6	0.003				3.32 ± 0.04	1.2 ± 0.9	0.007	6.7 ± 1.5	0.016
HA-As(III) *oxic*	0	1.76 ± 0.01	2.7 ± 0.1	0.003							9.1 ± 0.9	0.029
HA-Fe-As(III) *oxic*	57	1.71 ± 0.04	3.4 ± 0.3	0.003	2.90 ± 0.09	0.4 ± 0.5	0.007	3.30 ± 0.04	1.0 ± 1.0	0.007	9.4 ± 0.9	0.032
HA-Fe-As(V) *oxic*	100	1.70 ± 0.01	3.9 ± 0.2	0.003				3.33 ± 0.02	1.7 ± 0.6	0.007	7.3 ± 1.0	0.016
Bulk	70	1.71 ± 0.01	3.4 ± 1.0	0.003	2.82 ± 0.25	0.1 ± 0.4	0.007	3.37 ± 0.02	1.7 ± 0.6	0.007	7.1 ± 1.2	0.019
MapB Spot 1B	73	1.72 ± 0.01	3.6 ± 0.6	0.003	2.95 ± 0.04	0.7 ± 0.3	0.007	3.43 ± 0.06	0.8 ± 0.4	0.007	7.2 ± 1.4	0.013
MapB Spot 2B	65	1.71 ± 0.01	3.3 ± 0.3	0.004	2.88 ± 0.05	0.4 ± 0.5	0.007	3.40 ± 0.03	1.1 ± 1.4	0.007	6.3 ± 0.8	0.026
Zone1 Spot 7	89	1.70 ± 0.01	4.1 ± 0.6	0.003				3.28 ± 0.04	0.6 ± 1.0	0.005	2.8 ± 0.7	0.032

The amplitude reduction factor, S_o^2, was set to 1. [a]R(Å), interatomic distance; [b]N path degeneracy (coordination number); [c]The Debye-Weller parameters were homogenized around a mean value; [d]Energy-shift parameter; [e]R-factor =$\Sigma i(data_i\text{-}fit_i)^2/\Sigma idata$. The Debye-Weller for the Fe-Fe paths are covaried with σ^2As-Fe_1= σ^2As-Fe_2. The reported errors are determined by the fitting procedure. Multiple scattering MS1, MS2 and MS3 were included in As(V) predominant samples: MS1 = triangular As-O-O MS path, R = 1.8165 x $R_{As\text{-}O}$, $\sigma^2 = \sigma^2_{As\text{-}O}$; MS2 = collinear As-O-As-O MS path, R = 2 x $R_{As\text{-}O}$, σ^2 = 4 x $R_{As\text{-}O}$, $\sigma^2 = \sigma^2_{As\text{-}O}$, MS3 = non-collinear As-O-As-O MS path, R = 2 x $R_{As\text{-}O}$, σ^2 = 2 x $\sigma^2_{As\text{-}O}$

Table 4 Fe K-edge EXAFS fits for Fh, Lp and the HA-Fe-As complex along with the bulk and two spots of the natural sample.

	Fe-O1			Fe-O2			Fe-C			Fe-Fe1			Fe-Fe2			Fe-O_{distal}			Fe-Fe3				
Sample	R^a	N^b	σ^{2c}	R^a	N^b	σ^{2c}	R^a	N^b	σ^{2c}	R^a	N^b	σ^{2c}	R^a	N^b	σ^{2c}	R^a	N^b	σ^{2c}	R^a	N^b	σ^{2c}	$\Delta E(eV)^d$	R f
Fh-As(V)*oxic*	1.93±0.01	2.7±0.1	0	2.09±0.01	1.6±0.2	0				3.03±0.02	1.8±1.0	0.010	3.49±0.02	2.7±1.1	0.010	3.60±0.04	4.2±1.6	0.010				0.94±0.01	0.0
Lp-As(V)*oxic*	1.95±0.01	3.4±0.5	0	2.08±0.01	3.1±0.5	0				3.07±0.01	6.5±1.1	0.01				3.56±0.04	2.3±1.3	0.01	4.02±0.02	1.7±0.6	0.01	1.12±0.25	0.0
HA-Fe-As(III)*oxic*	1.94±0.03	3.1±1.6	0	2.06±0.05	2.2±1.5	0	2.97±0.02	1.8±0.6	0	3.11±0.05	0.2±0.8	0	3.44±0.2	1.0±1.4	0	3.57±0.01	1.4±0.2	0				0.80±0.40	0.0
Bulk	1.94±0.01	2.2±0.1	0	2.06±0.01	2.5±0.1	0	2.77±0.04	1.6±0.8	0.01	3.04±0.02	2.4±0.3	0.01				3.82±0.05	2.8±1.7	0.01	3.91±0.09	0.4±0.7	0.01	0.67±0.37	0.0
Spot 1	1.94±0.01	3.1±0.3	0	2.12±0.01	3.2±0.3	0				3.01±0.01	1.5±0.6	0				3.76±0.04	2.8±1.7	0	3.90±0.05	0.3±0.7	0	1.27±0.37	0.0
Spot 5	1.97±0.02	4.1±0.3	0	2.15±0.01	2.6±0.2	0				3.02±0.02	1.6±0.8	0.01				3.69±0.07	1.3±1.2	0.01	3.86±0.07	0.2±0.5	0.01	1.25±0.47	0.0

[a]R(Å), interatomic distance; [b]N, path degeneracy (coordination number); [c]σ^2(Å), Debye-Waller factor; [d]Energy-shift parameter; [e]R-factor =$\Sigma i(data_i\text{-}fit_i)^2/\Sigma idata$. The amplitude reduction factor, $S0^2$, was set to 0.75 from Fh fit. The reported errors are determined by the fitting procedure. Parameters were covaried as follows: σ^2Fe-O_1 = σ^2Fe-O_2 and σ^2Fe-$Fe_{1\text{-}2\text{-}3}$ = σ^2Fe-C = σ^2Fe-O_{distal}.